

Controllable Synchronization of Hierarchically Networked Oscillators

Jin Xu^{1,2}, Dong-Ho Park¹, and Junghyo Jo^{1,2,*}

¹Asia Pacific Center for Theoretical Physics, Pohang, Gyeongbuk 37673, Korea

²Department of Physics, Pohang University of Science and Technology, Pohang, Gyeongbuk 37673, Korea

E-mail: *jojunghyo@apctp.org

Abstract. The controllability of synchronization is an intriguing question in complex systems, in which hierarchically-organized heterogeneous elements have asymmetric and activity-dependent couplings. In this study, we introduce a simple and effective way to control synchronization in such a complex system by changing the complexity of subsystems. We consider three Stuart-Landau oscillators as a minimal subsystem for generating various complexity, and hierarchically connect the subsystems through a mean field of their activities. Depending on the coupling signs between three oscillators, subsystems can generate ample dynamics, in which the number of attractors specify their complexity. The degree of synchronization between subsystems is then controllable by changing the complexity of subsystems. This controllable synchronization can be applied to understand the synchronization behavior of complex biological networks.

PACS numbers: 05.45.Xt, 89.75.-k, 87.18.Gh

Keywords: Synchronization, Stuart-Landau model, Controllability, Complexity

1. Introduction

Synchronization of interacting elements is an emergent phenomenon in complex systems [1, 2, 3]. Rhythms and synchronization of neuronal activities are essential for odor discrimination [4], visual feature integration [5], and brain computation [6], but perfect synchronization is not always desirable, but can sometimes be disastrous in mental disorders such as epilepsy [7]. However, considering the enormous number of connections between cells and organs in the body, the apparent independence or desynchronization between rhythms in different organs may be a bigger puzzle rather than their synchronization [8]. Indeed electrical engineers design desynchronization to implement time division multiple access (TDMA) that prevents message collisions and provides asynchronous sleep cycles for nodes on wireless sensor networks [9]. Complex systems sometimes show partial synchronization. Two types of partial synchronization have been recognized. The *chimera state* shows spatial separation of synchronized and desynchronized domains [10], whereas the *periodic synchronization* shows temporal alternation between synchronized and desynchronized states [11, 12]. Unihemispheric sleep is an example of the chimera state where one half of the brain sleeps while the other half remains awake; some animals adopt this strategy when predation risk is high [13].

Context-dependent control of synchronization is therefore necessary to ensure that complex systems function appropriately. In particular, to disrupt synchronization and achieve desynchronization, various methods have been proposed; these include simply decreasing interaction strengths to stimulating with a short pulse [14], giving linear/nonlinear delayed feedback [15, 16, 17], and introducing inhibitory interactions [18]. Recent studies have investigated the synchronization-desynchronization transition in complex networks [19, 20]. These studies have revealed that in locally-coupled networks, this transition can be controlled by adapting the topology of networks [20]. However, those controls require parameter optimization, because the transition between synchronized and desynchronized states is sharp. On top of the fine-tuning problem, real systems generally have high complexities: (i) complex networks have heterogeneous couplings with excitatory and inhibitory links [21]; (ii) the strength of the couplings depends on the activities of nodes [22]; and (iii) the networks are hierarchically organized [23, 24, 25]. Therefore, precise control of synchronization looks implausible in complex systems.

We ask how such complex systems realize precise and robust control of synchronization between interacting elements. In a hierarchical system, generation of coherent behavior becomes increasingly difficult as the complexity of subsystems increases. This simple observation suggests a simple and effective way to control synchronization of a complex system by changing the *complexity* of its subsystems. Here we formulate a minimal model to demonstrate this idea by using coupled Stuart-Landau oscillators.

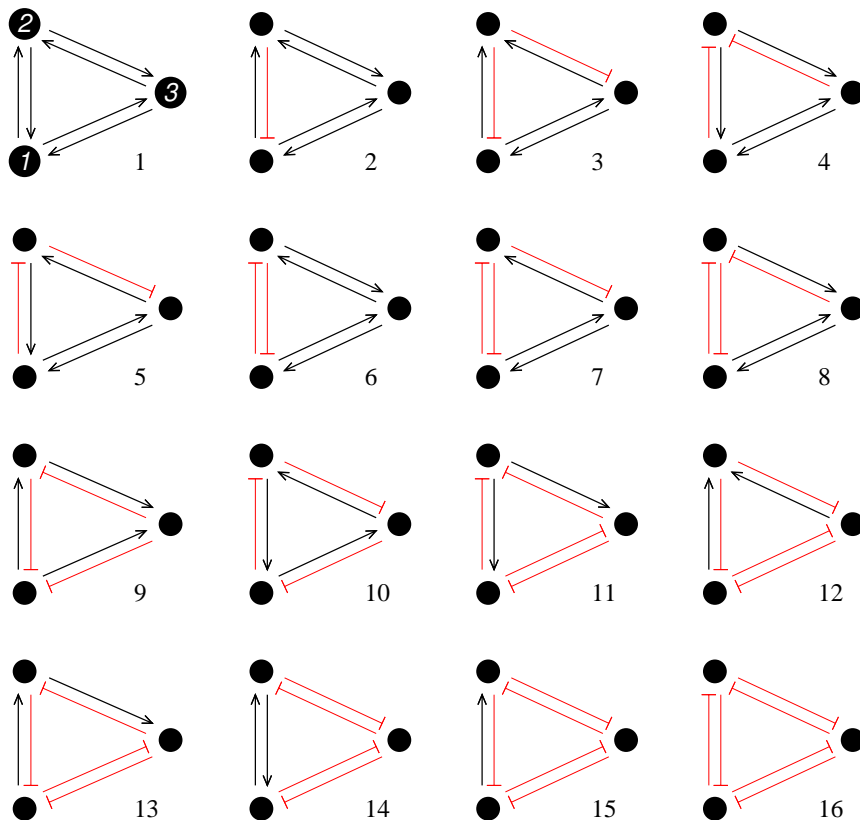


Figure 1. (Color online) Possible interactions between three oscillators. Black arrows: positive interactions; red bar-headed arrows: negative interactions.

2. Stuart-Landau oscillator

Synchronization phenomena can be generally described by considering oscillators and their coupling. In particular, we adopt Stuart-Landau oscillators in which amplitude and phase are variable [26]:

$$\dot{Z}_\sigma = (\lambda_\sigma - |Z_\sigma|^2 + i\omega_\sigma)Z_\sigma + K \sum_{\sigma' \neq \sigma} a_{\sigma\sigma'} Z_{\sigma'}. \quad (1)$$

First, we consider a *subsystem* that consists of three coupled oscillators with $\sigma, \sigma' \in \{1, 2, 3\}$ as a minimal set for generating diverse complexity. The dynamics of the complex variable $Z_\sigma \equiv r_\sigma e^{i\theta_\sigma}$ can be understood by decomposing amplitude and phase parts:

$$\dot{r}_\sigma = (\lambda_\sigma - r_\sigma^2)r_\sigma + K \sum_{\sigma' \neq \sigma} a_{\sigma\sigma'} r_{\sigma'} \cos(\theta_{\sigma'} - \theta_\sigma), \quad (2)$$

$$\dot{\theta}_\sigma = \omega_\sigma + K \sum_{\sigma' \neq \sigma} a_{\sigma\sigma'} \frac{r_{\sigma'}}{r_\sigma} \sin(\theta_{\sigma'} - \theta_\sigma). \quad (3)$$

In the absence of coupling ($K = 0$), the amplitude converges to a stable focus ($r_\sigma = 0$) for $\lambda_\sigma < 0$, but the focus loses stability at the Hopf bifurcation point ($\lambda_\sigma = 0$), and a stable limit-cycle emerges with amplitude $\sqrt{\lambda_\sigma}$ and frequency ω_σ for $\lambda_\sigma > 0$. Note that $r_\sigma = -\sqrt{\lambda_\sigma}$ is another solution for $\lambda_\sigma > 0$. Here we used only positive-definite

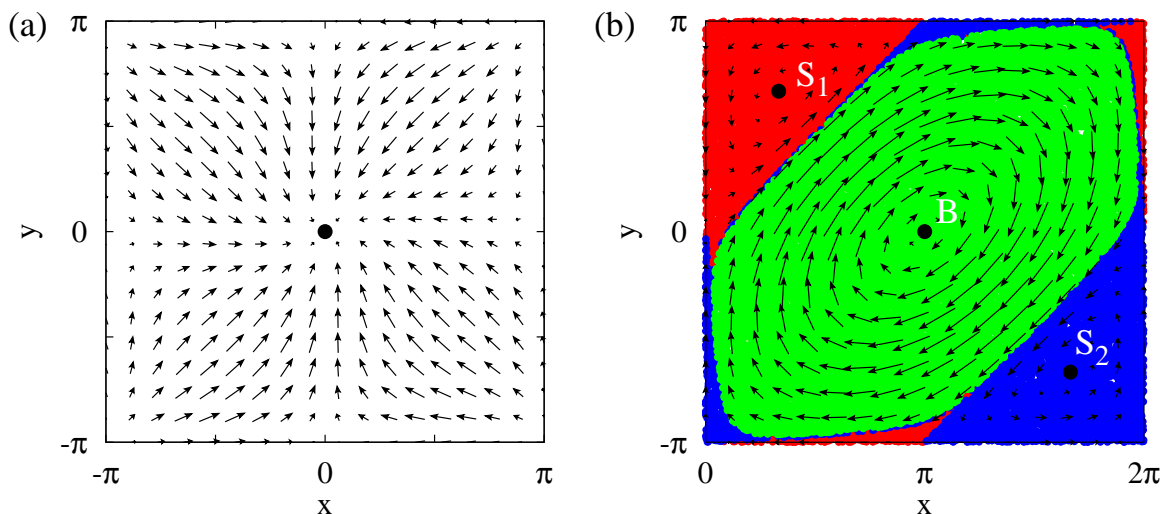


Figure 2. (Color online) Phase planes of the three coupled oscillators. (a) $\lambda_1 = 1.0$ and $\lambda_2 = \lambda_3 = 0.2$, and (b) $\lambda_1 = \lambda_2 = \lambda_3 = 1.0$. Black points: attractors; arrows: vector flows (\dot{x}, \dot{y}) on the plane (x, y) . (b) The basins of the three attractors, S_1 , S_2 , and B , are painted with red (top left), blue (bottom right), and green (middle), respectively.

r_σ ; when r_σ became negative in simulations, we made it positive with the following transformation, $r_\sigma = -r_\sigma$ and $\theta_\sigma = \theta_\sigma + \pi$.

Once the coupling is applied ($K > 0$), the subsystem produces ample dynamics depending on the adjacency matrix \mathbf{A} with entries $a_{\sigma\sigma'}$ that determine the coupling sign from oscillator σ' to oscillator σ . The phase part of Eq. (3) is a generalized Kuramoto model [26], in which oscillators have positive and negative couplings, and their coupling strengths depend on their amplitudes. The amplitude dependence has the physical meaning that when oscillator σ' affects oscillator σ , the coupling strength is proportional to the affecter amplitude $r_{\sigma'}$, but inversely proportional to the receiver amplitude r_σ ; i.e., the pair of strong affecter and weak receiver exhibits a maximal coupling.

When coupling is weak, the amplitudes can be approximated as $r_\sigma \approx \sqrt{\lambda_\sigma}$, and the three phase equations of Eq. (3) can be reduced to two equations of the phase differences, $x \equiv \theta_1 - \theta_2$ and $y \equiv \theta_1 - \theta_3$. Assuming identical intrinsic frequencies ($\omega_\sigma = w$) for simplicity, we obtain

$$\dot{x} = -(b_{12} + b_{21}) \sin x - b_{13} \sin y - b_{23} \sin(x - y), \quad (4)$$

$$\dot{y} = -b_{12} \sin x - (b_{13} + b_{31}) \sin y + b_{32} \sin(x - y), \quad (5)$$

where $b_{\sigma\sigma'} \equiv a_{\sigma\sigma'} K r_{\sigma'} / r_\sigma$. Their steady states ($\dot{x} = 0$ and $\dot{y} = 0$) are governed by the parameters λ_σ and the adjacency matrix \mathbf{A} . Here self-couplings can be safely ignored ($a_{\sigma\sigma} = 0$), because their contribution is absent in Eq. (3). Considering that the off-diagonal elements $a_{\sigma\sigma'}$ for $\sigma \neq \sigma'$ can take either 1 or -1 for positive or negative couplings, the adjacency matrix \mathbf{A} has a total of $64 (= 2^6)$ possibilities. Leaving index

degeneracy aside, 16 cases remain (Fig. 1). Most of them drive (x, y) to single attractors at steady states, regardless of λ_σ . However, two anti-symmetric matrices,

$$\mathbf{A} = \begin{pmatrix} 0 & -1 & -1 \\ 1 & 0 & -1 \\ 1 & 1 & 0 \end{pmatrix}, \begin{pmatrix} 0 & 1 & -1 \\ -1 & 0 & 1 \\ 1 & -1 & 0 \end{pmatrix},$$

which correspond to Networks 9 and 10 in Fig. 1, are exceptional in that they produce multiple attractors for similar λ_σ ($\lambda_1 \approx \lambda_2 \approx \lambda_3$). However, the two anti-symmetric matrices also generate single attractors for largely dissimilar λ_σ . The effective coupling $b_{\sigma\sigma'} \equiv a_{\sigma\sigma'}Kr_{\sigma'}/r_\sigma$ can be different from the topological coupling $a_{\sigma\sigma'}$ for largely dissimilar λ_σ . Therefore, we focus on Networks 9 and 10, which can alter their complexity (number of attractors) by controlling λ_σ . In particular, Network 9 has three populations of distinguishable oscillators: The first oscillator attracts the other two; the second repels the other two; and the third attracts one and repels one. In contrast, Network 10 has three populations of indistinguishable oscillators.

Network 9 produces single attractors for dissimilar λ_σ (Fig. 2a), but three attractors for similar λ_σ (Fig. 2b). For $\lambda_1 = \lambda_2 = \lambda_3 = 1$, the (x, y) phase plane has three attractors $(\pi/3, 2\pi/3)$, $(5\pi/3, -2\pi/3)$, and $(\pi, 0)$. We label them S_1 , S_2 , and B , because S_1 and S_2 have small basins of attractors, whereas B has a big basin (Fig. 2b). When initial conditions $[x(0), y(0)]$ are given in the small basins, the subsystem is quickly attracted to S_1 or S_2 , but when initial conditions are given in the big basin, the subsystem approaches B slowly; Near the center B , the change in the radius of the cycle is not readily apparent. When the amplitude dynamics in Eq. (2) is off ($\dot{r}_\sigma = 0$), and the phase model in Eq. (3) is only considered with frozen amplitudes, the subsystem is not attracted to the centers, but revolves endlessly around the centers at given initial radii [27]. S_1 , S_2 , and B are special positions in which the coupling terms, $\sum_{\sigma' \neq \sigma} a_{\sigma\sigma'}r_{\sigma'} \cos(\theta_{\sigma'} - \theta_\sigma) = 0$ in Eq. (2), vanish and amplitudes $r_\sigma = \sqrt{\lambda_\sigma}$ become fixed.

Network 10 has the same phase plane as Network 9, with simple translations $x \rightarrow x - \pi$ and $y \rightarrow y$.

3. Hierarchical Oscillators

To demonstrate that the synchronization of a hierarchical system can depend on the complexity (number of attractors) of subsystems, we construct a hierarchical system composed of multiple units. Each unit corresponds to one subsystem of the three coupled oscillators. The amplitude and phase of the oscillator σ in the n th unit are represented as $Z_{n\sigma} \equiv r_{n\sigma}e^{i\theta_{n\sigma}}$. We consider an *inter-unit* coupling in addition to the *intra-unit* coupling (Fig. 3a). In particular, we start by simply copying the intra-unit coupling into the inter-unit coupling:

$$\dot{Z}_{n\sigma} = (\lambda_\sigma - |Z_{n\sigma}|^2 + i\omega_{n\sigma})Z_{n\sigma} + K \sum_{\sigma' \neq \sigma} a_{\sigma\sigma'} Z_{n\sigma'} + \epsilon K \sum_{m \neq n} \sum_{\sigma' \neq \sigma} a_{\sigma\sigma'} Z_{m\sigma'}, \quad (6)$$

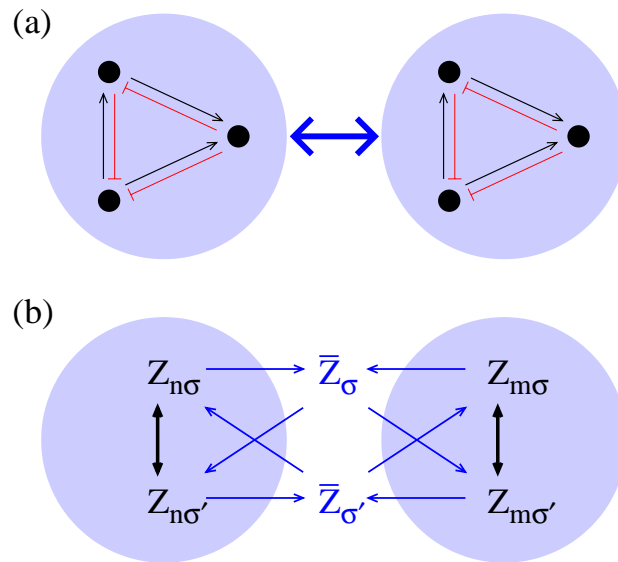


Figure 3. (Color online) Hierarchical organization of coupled oscillators. (a) Single units (blue filled circles) are composed of three coupled oscillators (black points), and the units interact with each other (thick blue arrow). (b) Each unit contributes to form mean fields \bar{Z}_σ , which then affect every unit in reverse.

where ϵ is introduced to represent weaker inter-unit couplings compared with intra-unit couplings ($0 < \epsilon < 1$). By using an arithmetic average of $Z_{n\sigma}$ for N units,

$$\bar{Z}_\sigma \equiv \frac{1}{N} \sum_{n=1}^N Z_{n\sigma}, \quad (7)$$

we can rearrange Eq. (6) as

$$\dot{Z}_{n\sigma} = (\lambda_\sigma - |Z_{n\sigma}|^2 + i\omega_{n\sigma})Z_{n\sigma} + \tilde{K} \sum_{\sigma' \neq \sigma} a_{\sigma\sigma'} (Z_{n\sigma'} + \tilde{\epsilon} \bar{Z}_{\sigma'}), \quad (8)$$

where $\tilde{K} = K(1 - \epsilon)$ and $\tilde{\epsilon} = N\epsilon/(1 - \epsilon)$. Henceforth, we use the rescaled parameters as $\tilde{K} \rightarrow K$ and $\tilde{\epsilon} \rightarrow \epsilon$. This equation can be interpreted as the mean fields \bar{Z}_σ affect every unit (Fig. 3b). To probe the inter-unit synchronization, we define order parameters for three populations of oscillators:

$$\rho_\sigma = \left| \frac{1}{N} \sum_{n=1}^N e^{i\theta_{n\sigma}} \right| \quad (9)$$

with $\sigma \in \{1, 2, 3\}$. Because three populations usually have the same degree of synchronization, hereafter, we represent them simply as ρ , unless otherwise specified. For the anti-symmetric intra-unit couplings, the arithmetic mean field leads to desynchronize units ($\rho = 0$), because the inter-unit coupling in Eq. (8) effectively generates repulsive interactions between units. For an example of two-unit systems ($N = 2$), $Z_{1\sigma}$ indirectly interacts with $Z_{2\sigma}$ through $Z_{2\sigma} \rightarrow Z_{2\sigma'} \rightarrow \bar{Z}_{\sigma'} \rightarrow Z_{1\sigma}$ or $Z_{1\sigma} \rightarrow Z_{1\sigma'} \rightarrow \bar{Z}_{\sigma'} \rightarrow Z_{2\sigma}$. These three-step interactions always yield a negative loop

as a net for the anti-symmetric matrices \mathbf{A} . The effective repulsion between units leads them to stay as far away as possible. This state has been referred as the *splay state* [20]. Therefore, under the arithmetic mean field, the anti-symmetric intra-unit coupling can provide an effective scheme for the desynchronization of hierarchical systems.

For the inter-unit coupling, we also consider a geometric average (log-average) of $Z_{n\sigma}$,

$$\bar{Z}_\sigma \equiv \bar{r}_\sigma e^{i\bar{\theta}_\sigma} = \left[\prod_{n=1}^N Z_{n\sigma} \right]^{1/N}. \quad (10)$$

The geometric average is frequently suitable in biological systems [28]. Unlike the arithmetic average in Eq. (7), the geometric average decouples amplitude and phase averages:

$$\bar{r}_\sigma \equiv \left[\prod_{n=1}^N r_{n\sigma} \right]^{1/N}, \quad (11)$$

$$\bar{\theta}_\sigma \equiv \frac{1}{N} \sum_{n=1}^N \theta_{n\sigma}. \quad (12)$$

The average phase $\bar{\theta}_\sigma$ is given as an arithmetic average of bare phases, independent on amplitudes. After adopting the geometric mean field \bar{Z}_σ of Eq. (10), we decompose Eq. (8) into amplitude and phase parts:

$$\dot{r}_{n\sigma} = (\lambda_\sigma - r_{n\sigma}^2)r_{n\sigma} + K \sum_{\sigma' \neq \sigma} a_{\sigma\sigma'} \left[r_{n\sigma'} \cos(\theta_{n\sigma'} - \theta_{n\sigma}) + \epsilon \bar{r}_{\sigma'} \cos(\bar{\theta}_{\sigma'} - \theta_{n\sigma}) \right], \quad (13)$$

$$\dot{\theta}_{n\sigma} = \omega_{n\sigma} + K \sum_{\sigma' \neq \sigma} a_{\sigma\sigma'} \left[\frac{r_{n\sigma'}}{r_{n\sigma}} \sin(\theta_{n\sigma'} - \theta_{n\sigma}) + \epsilon \frac{\bar{r}_{\sigma'}}{r_{n\sigma}} \sin(\bar{\theta}_{\sigma'} - \theta_{n\sigma}) \right]. \quad (14)$$

In this study, we adopt the geometric mean-field coupling, because it produces broader spectrum of synchronization between units. This completes our formulation of hierarchical oscillators.

4. Controlling synchronization

We investigate the synchronization of hierarchical oscillators governed by Eqs. (13) and (14). We first consider a two-unit system ($N = 2$), because it contains essential ingredients in the hierarchical system; then, we extend the model into large systems.

4.1. Two-unit system

To examine the dynamics of two-unit systems, we again focus on the phase differences ($x_{1,2}$ and $y_{1,2}$) between three oscillators within each unit, and the phase difference z between two units. The phase variables ($\theta_{11}, \theta_{12}, \theta_{13}, \theta_{21}, \theta_{22}, \theta_{23}$) of two units are transformed to (x_1, y_1, x_2, y_2, z) where $x_1 \equiv \theta_{11} - \theta_{12}$, $y_1 \equiv \theta_{11} - \theta_{13}$, $x_2 \equiv \theta_{21} - \theta_{22}$, $y_2 \equiv \theta_{21} - \theta_{23}$, and $z \equiv \theta_{11} - \theta_{21}$. Here we assume identical intrinsic frequencies ($\omega_{n\sigma} = \omega$) for simplicity.

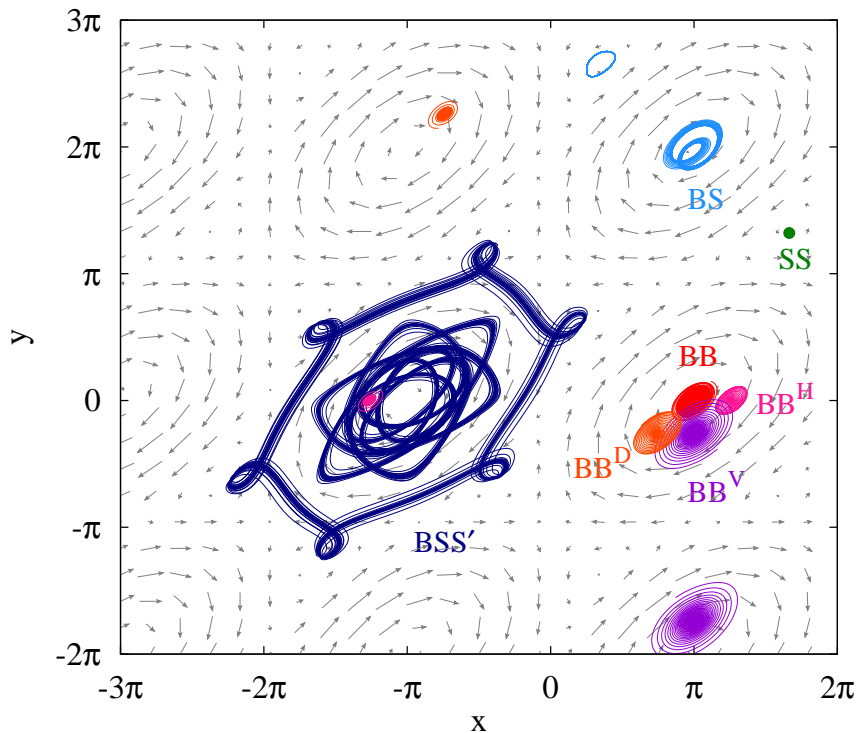


Figure 4. (Color online) Phase plane of two-unit systems. Under weak coupling ($K = 0.1$ and $\epsilon = 0.4$) and identical intrinsic frequencies ($\omega_{n\sigma} = 1$) for $\lambda_1 = \lambda_2 = \lambda_3 = 1$, the hierarchical system generates seven dynamic states: (i) SS state, in which two units are attracted into the same attractor S_1 or S_2 ; (ii) BS state, in which one unit rotates around S_1 or S_2 , and the other rotates around B ; (iii) BSS' state, in which one unit rotates around B , and the other unit jumps alternately between S_1 and S_2 . (iv) BB state, in which two units slowly approach B ; (v) BB^H ; (vi) BB^V ; (vii) BB^D states, in which two units slowly approach horizontally-, vertically-, and diagonally-shifted attractors from B . Different colors represent different pairs of two units.

First, when λ_σ are widely dissimilar, individual units have single and identical attractors (Section 2). Thus the phase differences (x_1, y_1) and (x_2, y_2) for two units are attracted into the same attractor in the absence of inter-unit coupling. The attraction is not perturbed even with weak coupling ($\epsilon = 0.4$) between units. Therefore, the inter-unit coupling contributes to fully synchronize the two units ($\rho = 1$).

Second, when λ_σ are similar (e.g., $\lambda_1 = \lambda_2 = \lambda_3 = 1$), individual units of Network 9 have three attractors (Fig. 2b), and two units can be attracted to different attractors (S_1, S_2, B). This complexity impedes the synchronization between the two units. In the absence of inter-unit coupling, the two units have four states if one considers the symmetry of S_1 and S_2 : (i) SS state, in which two units stay in the same small basin; (ii) SS' state, in which two units stay in different small basins. (iii) BS state, in which one unit stays in the big basin, while the other unit stays in one of the two small basins; and (iv) BB state, where two units stay in the big basin. Under weak inter-unit coupling ($\epsilon = 0.4$), we numerically solved Eqs. (13) and (14), and observed ample dynamics of

Table 1. State probability and synchronization of two-unit systems. The probabilities of eight states were obtained for the two-unit systems in the absence ($\epsilon = 0$) and presence ($\epsilon = 0.4$) of inter-unit coupling, given $\lambda_1 = \lambda_2 = \lambda_3 = 1$, $K = 0.1$, and $\omega_{n\sigma} = 1$. The order parameter ρ represents the degree of synchronization between two units. $\rho = 1$ means perfect synchronization; $\rho = 0$ means perfect desynchronization. We ran 10^4 different initial conditions to estimate the state probability and synchronization, and computed the standard deviation from 10 sets of ensembles to obtain their uncertainties.

X	$P(X \epsilon = 0)$	$\rho(\epsilon = 0)$	$P(X \epsilon = 0.4)$	$\rho(\epsilon = 0.4)$
SS	0.057 ± 0.001	0.6 ± 0.3	0.078 ± 0.003	1
SS'	0.057 ± 0.003	0.6 ± 0.3	0	-
BS	0.449 ± 0.005	0.6 ± 0.3	0.013 ± 0.001	0.6 ± 0.3
BSS'	0	-	0.245 ± 0.005	0.7 ± 0.3
BB	0.437 ± 0.004	0.6 ± 0.3	0.151 ± 0.005	0.8 ± 0.2
BB^H	0	-	0.208 ± 0.005	0.4
BB^V	0	-	0.154 ± 0.004	0.4
BB^D	0	-	0.152 ± 0.004	0.4

the two-unit system (Fig. 4):

- (i) SS state. Two units arrive at the same attractor, either S_1 or S_2 , and are fully synchronized ($\rho = 1$).
- (ii) SS' state. This state is unstable and excluded for $\epsilon = 0.4$. Therefore, two units never sit on S_1 and S_2 .
- (iii-1) BS state. Two units rotate around B and S_1/S_2 instead of being attracted into fixed points.
- (iii-2) BSS' state. One unit shows a precessional cycle around B , and the other unit jumps alternately between S_1 and S_2 .

When two units sit on different basins (BS and BSS' states), they show partial synchronizations ($0 < \rho < 1$). Regarding the BB state, we found new stationary solutions in the two-unit system that satisfy $r_{n\sigma} = \sqrt{\lambda_\sigma} = 1$ with no contribution of coupling terms in Eq. (13):

$$K \left[\cos x_1 + \cos y_1 \right] + \epsilon K \left[\cos \left(\bar{x} + \frac{z}{2} \right) + \cos \left(\bar{y} + \frac{z}{2} \right) \right] = 0, \quad (15)$$

$$K \left[\cos x_1 - \cos(x_1 - y_1) \right] + \epsilon K \left[\cos \left(x_1 - \frac{z}{2} \right) - \cos \left(x_1 - \bar{y} - \frac{z}{2} \right) \right] = 0, \quad (16)$$

$$K \left[\cos y_1 + \cos(x_1 - y_1) \right] + \epsilon K \left[\cos \left(y_1 - \frac{z}{2} \right) + \cos \left(\bar{x} - y_1 + \frac{z}{2} \right) \right] = 0, \quad (17)$$

$$K \left[\cos x_2 + \cos y_2 \right] + \epsilon K \left[\cos \left(\bar{x} - \frac{z}{2} \right) + \cos \left(\bar{y} - \frac{z}{2} \right) \right] = 0, \quad (18)$$

$$K \left[\cos x_2 - \cos(x_2 - y_2) \right] + \epsilon K \left[\cos \left(x_2 + \frac{z}{2} \right) - \cos \left(x_2 - \bar{y} + \frac{z}{2} \right) \right] = 0, \quad (19)$$

$$K \left[\cos y_2 + \cos(x_2 - y_2) \right] + \epsilon K \left[\cos \left(y_2 + \frac{z}{2} \right) + \cos \left(\bar{x} - y_2 - \frac{z}{2} \right) \right] = 0 \quad (20)$$

with $\bar{x} \equiv (x_1 + x_2)/2$ and $\bar{y} \equiv (y_1 + y_2)/2$. Under these constraints, Eq. (14) yields five phase difference equations:

$$\begin{aligned} \dot{x}_1 = & K \left[\sin y_1 + \sin(x_1 - y_1) \right] \\ & + \epsilon K \left[\sin \left(\bar{x} + \frac{z}{2} \right) + \sin \left(\bar{y} + \frac{z}{2} \right) - \sin \left(x_1 - \frac{z}{2} \right) + \sin \left(x_1 - \bar{y} - \frac{z}{2} \right) \right], \end{aligned} \quad (21)$$

$$\begin{aligned} \dot{y}_1 = & K \left[\sin x_1 + \sin(x_1 - y_1) \right] \\ & + \epsilon K \left[\sin \left(\bar{x} + \frac{z}{2} \right) + \sin \left(\bar{y} + \frac{z}{2} \right) - \sin \left(y_1 - \frac{z}{2} \right) + \sin \left(\bar{x} - y_1 + \frac{z}{2} \right) \right], \end{aligned} \quad (22)$$

$$\begin{aligned} \dot{x}_2 = & K \left[\sin y_2 + \sin(x_2 - y_2) \right] \\ & + \epsilon K \left[\sin \left(\bar{x} - \frac{z}{2} \right) + \sin \left(\bar{y} - \frac{z}{2} \right) - \sin \left(x_2 + \frac{z}{2} \right) + \sin \left(x_2 - \bar{y} + \frac{z}{2} \right) \right], \end{aligned} \quad (23)$$

$$\begin{aligned} \dot{y}_2 = & K \left[\sin x_2 + \sin(x_2 - y_2) \right] \\ & + \epsilon K \left[\sin \left(\bar{x} - \frac{z}{2} \right) + \sin \left(\bar{y} - \frac{z}{2} \right) - \sin \left(y_2 + \frac{z}{2} \right) + \sin \left(\bar{x} - y_2 - \frac{z}{2} \right) \right], \end{aligned} \quad (24)$$

$$\begin{aligned} \dot{z} = & K \left[\sin x_1 + \sin y_1 - \sin x_2 - \sin y_2 \right] \\ & + \epsilon K \left[\sin \left(\bar{x} + \frac{z}{2} \right) - \sin \left(\bar{x} - \frac{z}{2} \right) + \sin \left(\bar{y} + \frac{z}{2} \right) - \sin \left(\bar{y} - \frac{z}{2} \right) \right]. \end{aligned} \quad (25)$$

We examine the stationary conditions, $\dot{x}_1 = \dot{y}_1 = \dot{x}_2 = \dot{y}_2 = \dot{z} = 0$. It is interesting that $\dot{x}_2 = \dot{y}_2 = 0$ is automatically satisfied, once $\dot{x}_1 = \dot{y}_1 = 0$ with constraints, $\bar{x} = \{0, \pi\}$ and $\bar{y} = \{0, \pi\}$. The condition gives four BB states:

(iv-1) BB state ($\bar{x} = \pi$ and $\bar{y} = 0$). Two units arrive at B ($x_1 = x_2 = \pi$ and $y_1 = y_2 = 0$) with arbitrary phase difference z between two units. Any z values can satisfy $\dot{z} = 0$ in Eq. (25); i.e., two units are coupled, but still behave independently.

(iv-2) BB^H state ($\bar{x} = 0$ and $\bar{y} = 0$). Two units (x_1, y_1) and (x_2, y_2) are horizontally located from their center $(0, 0)$; $y_1 = y_2 = 0$, and $x_1 (= -x_2)$ and z satisfy

$$e^{ix_1} + 2\epsilon e^{iz/2} = -1. \quad (26)$$

(iv-3) BB^V state ($\bar{x} = \pi$ and $\bar{y} = \pi$). Two units (x_1, y_1) and (x_2, y_2) are vertically located from their center (π, π) ; $x_1 = x_2 = \pi$, and $y_1 (= 2\pi - y_2)$ and z satisfy

$$e^{iy_1} - 2\epsilon e^{iz/2} = 1. \quad (27)$$

(iv-4) BB^D state ($\bar{x} = 0$ and $\bar{y} = \pi$). Two units (x_1, y_1) and (x_2, y_2) are diagonally located from their center $(0, \pi)$; $x_1 - y_1 = -\pi$, and $y_1 (= 2\pi - y_2)$ and z satisfy

$$e^{iy_1} + 2\epsilon e^{i(y_1 - z/2)} = 1. \quad (28)$$

The complex Eqs. (26)-(28) give exact values of the phase differences (x_1, y_1) and (x_2, y_2) between three oscillators within each unit, and the phase difference z between two units. However, if ϵ is too small, they do not have solutions. Therefore, BB^H , BB^V , and BB^D states can only emerge under sufficient inter-unit coupling. For $\epsilon = 0.4$, the three states show partial synchronization ($\rho = 0.4$). The realization of these seven states depends on initial conditions, $[r_{n\sigma}(0), \theta_{n\sigma}(0)]$. However, the initial-condition dependence is chaotic

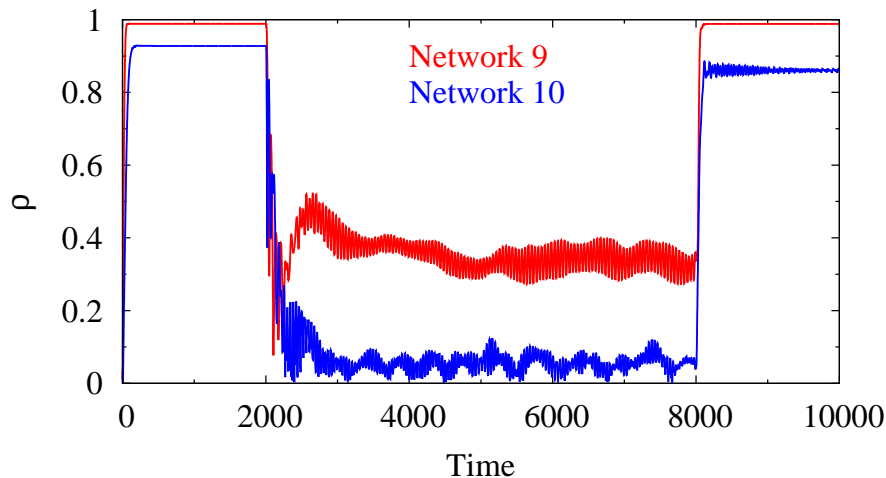


Figure 5. (Color online) Control of synchronization. The synchronization between 1000 units is controlled by adjusting the complexity of individual units through λ_σ . Given Network 9 (red) and Network 10 (blue), single attractors are generated for dissimilar λ_σ ($\lambda_1 = 1.0$ and $\lambda_2 = \lambda_3 = 0.2$), while three attractors are generated for similar λ_σ ($\lambda_1 = \lambda_2 = \lambda_3 = 1.0$). The dissimilar λ_σ is changed to the similar λ_σ at $t = 2000$, and back to the dissimilar λ_σ at $t = 8000$. For the simulation, coupling parameters were set to $K = 0.1$ and $\epsilon = 0.4$, and uniformly-distributed intrinsic frequencies were used as $\omega_{n\sigma} \in [0.99, 1.01]$.

in the two-unit system. Although we can not predict final states given initial conditions, the realization probability of each state is not uncertain (Table 1). The probability of SS state, which generates full synchronization ($\rho = 1$), is relatively small because the probability is small that two units will enter the same small basin. Therefore, as the number of units considered increases, the likelihood that each unit sits on a different attractor also increases, so the units in a hierarchical system may become partially synchronized.

We performed the same analysis for Network 10, and confirmed that the two-unit system of Network 10 also generates seven states like Network 9. Their realization probabilities are also the same except for the switch between BB and BB^H states: $P(BB|\text{Network10})=P(BB^H|\text{Network9}) \approx 0.21$ and $P(BB^H|\text{Network10})=P(BB|\text{Network9}) \approx 0.15$.

4.2. Multi-unit system

We now consider a hierarchical system that is composed of a large number of subsystems ($N > 2$). When the system is sufficiently large ($N = 1000$), it produces homogeneous synchronization patterns, independent of initial conditions, unlike the two-unit system. However, like the two-unit system, we could control the synchronization of the large system simply by changing the complexity (number of attractors) of subsystems by adjusting λ_σ (Fig. 5). For largely dissimilar λ_σ , individual units have single attractors,

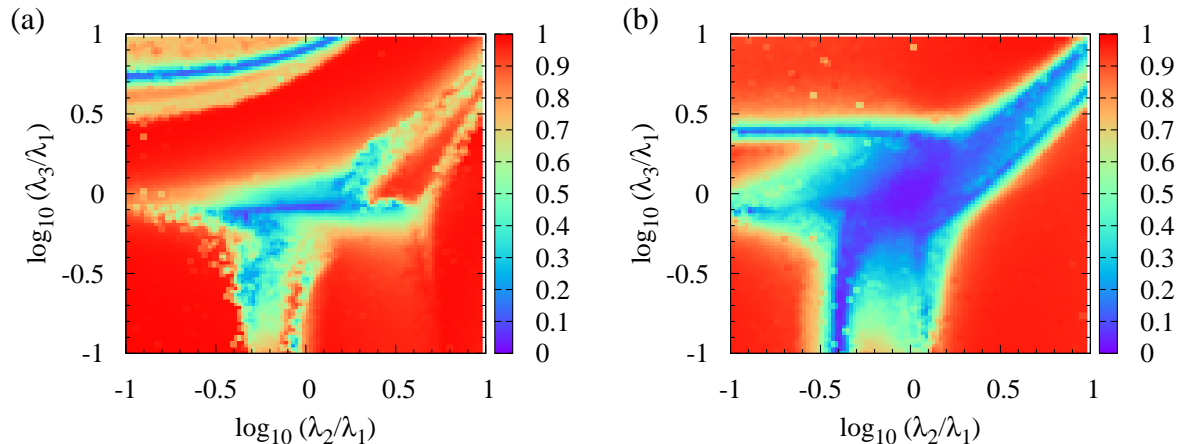


Figure 6. (Color online) Parameter dependence of synchronization. Given λ_2/λ_1 and λ_3/λ_1 , the degree of synchronization between 1000 units is recorded for a long period after equilibration. Its time average $\langle \rho_1 \rangle$ is represented by colors (blue: desynchronization; red: synchronization). (a) Network 9 and (b) Network 10. Axes have base-10-logarithmic scales to allow presentation of a large range of λ_σ . For the simulation, coupling parameters were set to $K = 0.1$ and $\epsilon = 0.4$, and uniformly-distributed intrinsic frequencies were used as $\omega_{n\sigma} \in [0.99, 1.01]$.

and thus become easily synchronized ($\rho = 1$). In contrast, similarity of λ_σ increases, it becomes more probable that they will enter basins of different attractors. This circumstance leads to partial synchronization or desynchronization of units ($0 \leq \rho \ll 1$). Network 9 was slightly more effective for synchronization, but slightly less effective for desynchronization than Network 10. This result is similar to the observation that in the two-unit system, Network 10 had a higher probability than Network 9 of generating the BB state, in which individual units behave independently despite the inter-unit interaction.

To check the robustness of controllability, we examined how parameters λ_σ affect the degree of synchronization. We obtained similar degrees of synchronization over large ranges of λ_σ (Fig. 6). This demonstrates robust control of synchronization based on changes of the number of attractors, not based on changes of the attractor positions.

5. Summary

We introduced a simple and effective way to control synchronization between elements in complex systems, in which hierarchically-organized heterogeneous elements have asymmetric and activity-dependent couplings. We formulated this idea by using Stuart-Landau oscillators. Each subsystem consisted of three oscillators that interacted to each other positively or negatively. Anti-symmetric couplings between three oscillators were special to generate single and multiple dynamic attractors depending on the amplitudes of the oscillators. Here the number of attractors could specify the complexity of subsystems. When the subsystems were connected through a mean field of their

average activities, the degree of synchronization between subsystems was controllable by changing the complexity of subsystems. In particular, we considered two kinds of mean fields using arithmetic average and geometric average, and found that the geometric mean field that counts large outliers less important was effective for controlling synchronization.

The controllable synchronization can be applied to understand the synchronization behavior of complex biological networks. Interestingly, anti-symmetric couplings of three populations (Network 9) are realized in pancreatic islets [29], and the synchronization between pancreatic islets is an important requirement in glucose metabolism [30]. Our finding may help to understand how islet-cell networks are synchronized.

Acknowledgements

This research was supported by Basic Science Research funded by Ministry of Science, ICT & Future Planning No. 2013R1A1A1A1006655 and by the Max Planck Society, the Korea Ministry of Education, Science and Technology, Gyeongsangbuk-Do and Pohang City.

- [1] Y. Kuramoto, *Chemical Oscillations, Waves, and Turbulence* (Springer, Berlin, 1984).
- [2] A. Pikovsky, M. Rosenblum, and J. Kurths, *Synchronization: a universal concept in nonlinear sciences* (Cambridge University Press, Cambridge, 2001).
- [3] S.H. Strogatz, *Sync: how order emerges from chaos in the universe, nature, and daily life* (Hachette Books, , 2004).
- [4] M. Stopfer, S. Bhagavan, B.H. Smith, and G. Laurent, *Nature* **390**, 70 (1997).
- [5] W. Singer and C.M. Gray, *Annu. Rev. Neurosci.* **18**, 555 (1995).
- [6] A.K. Engel, P. Fries, and W. Singer, *Nat. Rev. Neurosci.* **2**, 704 (2001).
- [7] R. Jiruska, M. de Curtis, J.G.R. Jefferys, *J. Physiol.* **591**, 787 (2013).
- [8] L. Glass, *Nature* **410**, 277 (2001).
- [9] J. Degeysys, I. Rose, A. Patel, and R. Nagpal, *International Conference on Information Processing in Sensor Networks* (2007).
- [10] D.M. Abrams and S.H. Strogatz, *Phys. Rev. Lett.* **93**, 174102 (2004).
- [11] M.Y. Choi, Y.W. Kim, and D.C. Hong, *Phys. Rev. E* **49**, 3825 (1994).
- [12] H. Hong, *Phys. Rev. E* **89**, 062924 (2014).
- [13] N.C. Rattenborg, S.L. Lima, and C.J. Amlaner, *Nature* **397**, 397 (1999).
- [14] Y. Zhai, I.Z. Kiss, P.A. Tass, and J.L. Hudson, *Phys. Rev. E* **71**, 065202 (R) (2005).
- [15] M.G. Rosenblum and A.S. Pikovsky, *Phys. Rev. Lett.* **92**, 114102 (2004).
- [16] C.-U. Choe, T. Dahms, P. Hövel, and E. Schöll, *Phys. Rev. E* **81**, 025205 (R) (2010).
- [17] O.V. Popovych, C. Hauptmann, and P.A. Tass, *Phys. Rev. Lett.* **94**, 164102 (2005).
- [18] V.H.P. Louzada, N.A.M. Araújo, J.S. Andrade Jr., and H.J. Herrmann, *Sci. Rep.* **2**, 658 (2012).
- [19] C. Wille, J. Lehnert, and E. Schöll, *Phys. Rev. E* **90**, 032908 (2014).
- [20] J. Lehnert, P. Hövel, A. Selivanov, A. Fradkov, and E. Schöll, *Phys. Rev. E* **90**, 042914 (2014).
- [21] C.Börgers and N. Kopell, *Neural Computation* **15**, 509 (2003).
- [22] V.P. Zhitulin, M.I. Rabinovich, R. Huerta, and H.D.I. Abarbanel, *Phys. Rev. E* **67**, 021901 (2003).
- [23] C. Zhou, L. Zemanová, G. Zamora, C.C. Hilgetag, and J. Kurths, *Phys. Rev. Lett.* **97**, 238103 (2006).
- [24] A. Pikovsky and M. Rosenblum, *Phys. Rev. Lett.* **101**, 264103 (2008).
- [25] Y. Kawamura, *Sci. Rep.* **4**, 4832 (2014).

- [26] J.A. Acebron *et al.*, Rev. Mod. Phys. **77**, 137 (2005).
- [27] H. Hong, J. Jo, and S.-J. Sin, Phys. Rev. E **88**, 032711 (2013).
- [28] F. Galton, Proc. R. Soc. Lond. **29**, 365 (1879).
- [29] T. van der Meulen, C.J. Donaldson, E. Cáceres, A.E. Hunter, C. Cowing-Zitron, L.D. Pound, M.W. Adams, A. Zembrzycki, K.L. Grove, and M.O. Husing, Nat. Med. **21**, 769 (2015).
- [30] M.G. Pedersen, R. Bertram, and A. Sherman, Biophys. J. **89**, 107 (2005).